# Conformal TCO-semiconductor-metal nanowire array for narrowband and polarization-insensitive hot-electron photodetection application

Zhang, Cheng; Wu, Kai; Ling, Bo; Li, Xiaofeng

2016

Zhang, C., Wu, K., Ling, B., & Li, X. (2016). Conformal TCO-semiconductor-metal nanowire array for narrowband and polarization-insensitive hot-electron photodetection application. Journal of Photonics for Energy, 6(4), 042502-. doi:10.1117/1.JPE.6.042502

https://hdl.handle.net/10356/89995

https://doi.org/10.1117/1.JPE.6.042502

Journal of Photonics for Energy

PhotonicsforEnergy.SPIEDigitalLibrary.org

# Conformal TCO-semiconductor-metal nanowire array for narrowband and polarization-insensitive hot-electron photodetection application

Cheng Zhang
Kai Wu
Bo Ling
Xiaofeng Li

SPIE.

Cheng Zhang, Kai Wu, Bo Ling, Xiaofeng Li, "Conformal TCO-semiconductor-metal nanowire array for narrowband and polarization-insensitive hot-electron photodetection application," *J. Photon. Energy* **6**(4), 042502 (2016), doi: 10.1117/1.JPE.6.042502.

# Conformal TCO-semiconductor-metal nanowire array for narrowband and polarization-insensitive hot-electron photodetection application

**Cheng Zhang,[a,b] Kai Wu,[a,b] Bo Ling,[c] and Xiaofeng Li[a,b,*]**

[a]Soochow University, College of Physics, Optoelectronics and Energy and Collaborative Innovation Center of Suzhou Nano Science and Technology, No 1, Shizi Street, Gusu District, Suzhou 215006, China

[b]Soochow University, Key Lab of Advanced Optical Manufacturing Technologies of Jiangsu Province and Key Lab of Modern Optical Technologies of Education Ministry of China, No 1, Shizi Street, Gusu District, Suzhou 215006, China

[c]Nanyang Technological University, Division of Microelectronics, School of Electrical and Electronic Engineering, 50 Nanyang Avenue, 639798, Singapore

**Abstract.** The use of hot electrons arising from the nonradiative decay of surface plasmons (SPs) is increasingly attracting interests in photodetection, photovoltaics, photocatalysis, and surface imaging. Nevertheless, the quantum efficiency of the hot-electron devices has to be improved to promote the practical applications. We propose an architecture of conformal TCO/semiconductor/metal nanowire (NW) array for hot-electron photodetection with a tunable optical response across the visible and near-infrared bands. The wavelength, strength, and bandwidth of the plasmonic resonance are tailored by controlling the lattice periodicity and topology. Finite-element simulation demonstrates that the near-perfect, polarization-insensitive, and ultranarrow-band optical absorption can be achieved in the conformal NW system. By the excitation of localized SPs, a strong field concentrates at the top corner of the NWs with a high hot-electrons generation rate. The analytical probability-based electrical calculation further shows that the SPs-enhanced photoresponsivity can be more than five times larger than that of the flat reference. © *2016 Society of Photo-Optical Instrumentation Engineers (SPIE)* [DOI: 10.1117/1.JPE.6.042502]

**Keywords:** hot electrons; photodetector; localized surface plasmons; photoresponsivity.

Paper 16038SS received Apr. 12, 2016; accepted for publication May 26, 2016; published online Jul. 12, 2016.

## 1 Introduction

Hot electrons directly generated from the nonradiative decay of surface plasmons (SPs) can be harnessed to enable a broad range of applications, such as photodetection,[1–13] photovoltaics,[14,15] photocatalysis,[16,17] and surface imaging.[18,19] In terms of photodetection, hot-electron photodetectors have the advantages in detecting the light with energy well below the semiconductor band edge, room-temperature operation, and highly controllable resonant wavelength. In 2011, the active nanoantenna that unites the light harvesting and conversion was reported to extend the spectral response to photon energies slightly higher than the Schottky barrier height, breaking the band limitation of Si material.[1] The new concept of hot-electron photodetectors is further demonstrated in various metallic nanostructures including nanorods,[2] nanowires (NWs),[3] gratings,[4–6] and waveguides.[7] However, for an alternative approach of hot electron collection based on the metal–insulator–metal (MIM) junctions, the efficiency of hot electron generation still remains low. Recently, the improved photoemission of hot electrons has been demonstrated by exciting the SPs within a planar MIM device,[8] and structuring one of the metallic contacts into a plasmonic strip was explored to enhance light absorption in the near-surface region.[9] Our previous study showed that the multilayered conformal grating can lead to a strong and highly

*Address all correspondence to: Xiaofeng Li, E-mail: xfli@suda.edu.cn

asymmetrical optical absorption between the top and bottom metal layers and therefore improves the responsivity by three times of that based on the conventional grating system.[10]

For high-performance photodetection application, the characteristics of high, tunable, polarization-insensitive, and narrowband photoresponse are urgently desired. In this study, we propose the plasmonic hot-electron photodetectors under the periodic configuration consisted of conformal TCO/semiconductor/metal (TCO/S/M, TCO: transparent conductive oxide) NWs. The symmetrical design ensures a perfect polarization-insensitivity of the device, fulfilling a key requirement for practical photodetection technology.[5] Because the semiconductor used here is intrinsic, the device behaves as a modified MIM structure and therefore is substantially different from the conventional Schottky junction formed at the metal/semiconductor interface (where the semiconductor normally highly doped). The main benefit through replacing insulator with the wide-bandgap semiconductor is the decreased barrier height ($\Phi_B$), which extends the detectable wavelength range, increases the tunneling probability through the semiconductor, and thus improves the photoresponsivity. Due to the low absorption coefficient of TCO, the parasitic absorption in the contrary electrode is minimal, therefor the metal on the other side is replaced. In the conformal NWs, the metal is periodically corrugated, which excites tunable SP resonances across the visible and near-infrared (NIR) by controlling the periodicity and topology of NW array.[11] The interaction of incident light with the nanostructured metal generates a strong electric field within the near field, therefore improves the optical absorption. Electromagnetic simulation further predicts a near-perfect optical absorption in the metallic cladding layer under plasmonic resonances, contributing to a high efficiency of hot electron photoemission and large unidirectional photocurrent. In addition, the full width at half maximum (FWHM) is as narrow as 5 nm (7.4 meV) at the resonance of $\lambda = 913$ nm, which is even half narrower compared with the previous report.[10] The analytical probability-based electrical calculation shows that the SPs-enhanced photoresponsivity can be up to 56 nA/mW (unbiased), which is more than five times larger than that of the planar reference (11 nA/mW).

## 2 Device Configuration and Method

The schematic diagram of the conformal NW array hot-electron photodetector as well as the side and cross-sectional views of one NW unit are shown in Figs. 1(a)–1(c). The device is composed of a two-dimensional (2-D) square array (with period $\Lambda$) of conformally configured NWs, which have the indium-doped tin oxide (ITO) cylinder core (with radius $r$), the ultrathin zinc oxide

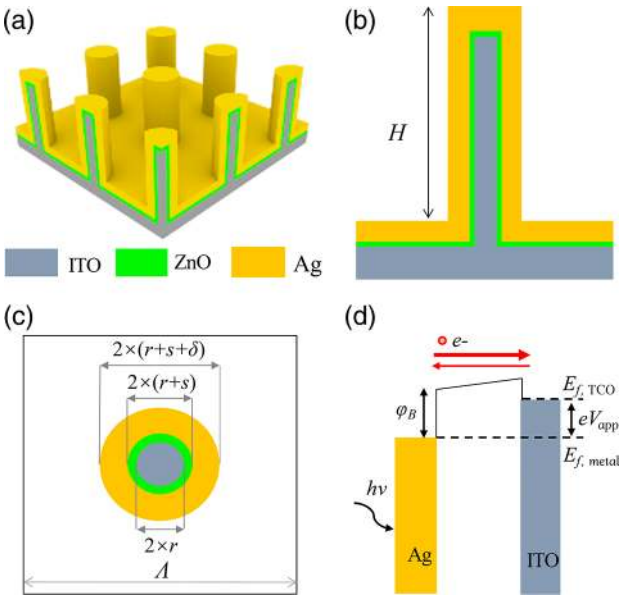


**Fig. 1** The schematic diagram of (a) the conformal NW array hot-electron photodetector, (b) side and (c) cross-sectional views of one NW unit. (d) Energy band diagram for the TCO/S/M barrier structure under a bias of $V_{app}$.

(ZnO) shell (with thickness $s = 4$ nm), and the silver cladding layer (with thickness $\delta = 60$ nm) on the ITO substrate. Here, $s = 4$ nm is used to ensure a high probability for the generated hot electrons in metal layers to tunnel through the ultrathin semiconductor intermediate layer. The NW depth is set to be $H = 500$ nm, in order to excite the localized SP modes.[13]

Figure 1(d) shows the band diagram of the TCO/S/M junction under a bias of $V_{app}$, in which $E_{f,metal}$ ($E_{f,TCO}$) and $\varphi_B$ are the Fermi level of Ag (ITO) and the barrier height (~0.6 eV) for Ag/ZnO interface,[20,21] respectively. Once the SPs are excited, the incident electromagnetic energy is efficiently coupled into the plasmonic system, generating hot electrons in the metal layer. The hot electron cannot be generated in the ITO due to its relatively low electron concentration in the considered photon energy range.[15] For hot electrons with energies exceeding the M/S band offset, they have the probabilities to (1) diffuse to the M/S interface without losing energy in an inelastic collision, (2) climb across the M/S barrier, (3) travel through the semiconductor without inelastic collisions, and (4) be collected by the bottom ITO contact. Nevertheless, for hot electrons with energies below the barrier height, the tunneling probability is much smaller according to the Wentzel–Kramers–Brillouin calculation, contributing to the neglectable photocurrent.[8]

Based on the optical constants from Palik,[22] the optical response of the proposed conformal NWs under normal incidence is analyzed in detail by solving the Maxwell equations via the full-wave finite-element method.[23] The electrical performance of the photodetectors is evaluated by the analytical probability-based calculation using the optically resolved electron generation profile.[9,10]

## 3 Optoelectronic Performance

We first examine the possibility of realizing a high and narrow-band light harvesting as well as the resonance tunability for hot-electron photodetection across various spectral bands in terms of the conformal NW array design. It should be noted that the overall optical performance is regulated by the net absorption of the device ($P_{net}$), which is the absorption difference by the cladding Ag and the core ITO layers ($P_{net} = P_{Ag} - P_{ITO}$). $P_{net}$ map versus the incident wavelength and the NW period is given in Fig. 2(a), where a relatively small ITO core is considered ($r = 20$ nm). It is clear that: (1) $P_{net}$ under resonance can be extremely high (close to 100%), showing that the

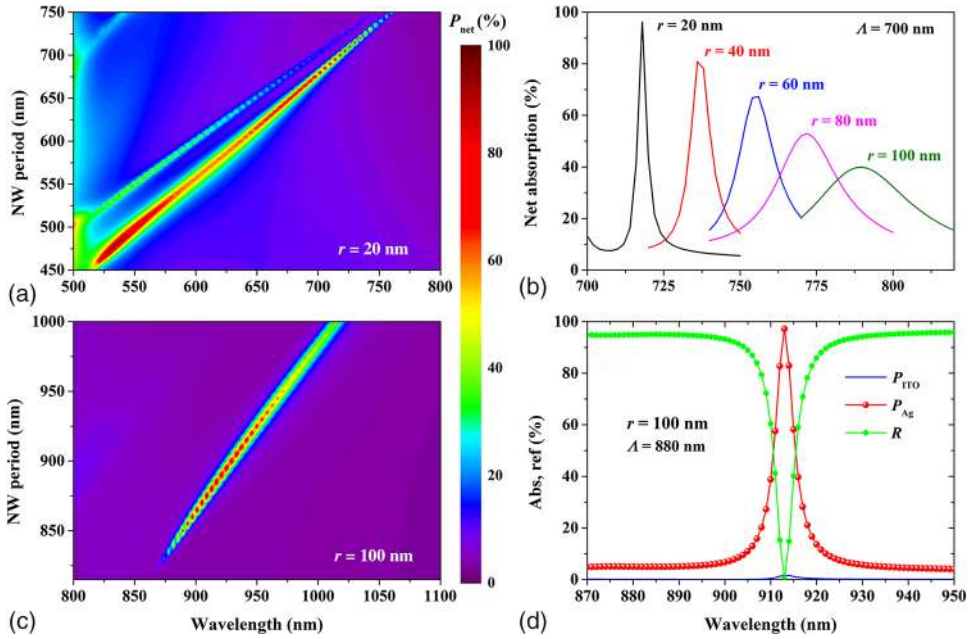


**Fig. 2** The contour maps of net absorption as a function of the incident wavelength and NW period $\Lambda$ with (a) $r = 20$ nm and (c) $r = 100$ nm. (b) The net absorption spectra for $r$ from 20 to 100 nm with $\Lambda = 700$ nm. (d) The detailed optical absorption and reflection responses in the conformal NWs with $r = 100$ nm and $\Lambda = 880$ nm.

Ag cladding can absorb nearly all the electromagnetic energy under plasmonic resonance; (2) a weak hybrid plasmon mode appears at shorter wavelength of the strong plasmonic resonance;[24,25] (3) the plasmonic resonance can be tuned readily by adjusting the NW period,[26] i.e., a larger NW separation enables a longer-wavelength photodetection. However, Fig. 2(a) also exhibits that solely adjusting the NW period can hardly obtain the constantly high $P_{net}$, which is gradually degraded with increasing $\Lambda$. Plotted in Fig. 2(b) exhibits that the plasmonic resonance can also be controlled by varying the ITO core radius $r$, i.e., a larger ITO core redshifts the resonance, however, it is accompanied with the broadened and weakened absorption peak. Therefore, a more reliable design should be based on controlling both the period as well as the NW size simultaneously.

Employing a large $r = 100$ nm, $P_{net}$ map versus the wavelength and $\Lambda$ is re-examined in Fig. 2(c), which illustrates a strong and extremely narrow plasmonic band again, but occurring at the longer-wavelength region. For example, under $\Lambda = 880$ nm and $r = 100$ nm, Fig. 2(d) indicates the spectral responses of the Ag absorption, the ITO absorption, and the device overall reflection. It is found that: (1) under resonance, 97.2% of the incident light is absorbed by the Ag layer and the parasitic absorption by ITO is tiny, leading to a highly efficient photoemission of hot electrons; (2) the reflection loss of the device is negligible under resonance, while it can be ~95% for off-resonance situations since the whole device surface is covered by the Ag layer; (3) the FWHM of the conformal NW hot-electron photodetector is ~5 nm (7.4 meV), which is even half narrower compared with the previous report.[10]

To better understand the plasmonic resonance nature as well as its contribution to the generation and collection processes of hot electrons in the conformal NW photodetector, it is necessary to examine the spatial characteristics of the hot-electron generation rate ($G$), which is defined as[27]

$$G(x, y, z, \omega) = \varepsilon_i |E(x, y, z, \omega)|^2 / (2\hbar), \tag{1}$$

where one absorbed photon is assumed to excite one electron-hole pair, $\varepsilon_i$ is the imaginary part of dielectric permittivity, $\omega$ is the angular frequency of incident light, $E$ is the electric field at position $(x, y, z)$, and $\hbar$ is the reduced Planck constant.

Figure 3(a) illustrates the three-dimensional (3-D) spatial distribution of $G$ in one unit of the conformal NW hot-electron photodetector, where the system parameters are inherited from Fig. 2(d) and the incident light is polarized along the $x$ axis. It is clear that most hot electrons are generated in the locations close to the top part of NWs, revealing a strong field concentration resulting from the excitation of localized SPs.[11] To unveil the spatial generation profile inside the NWs, the corresponding cross-sectional generation pattern in the $yz$ plane is shown in Fig. 3(b). We observe the highest $G$ at the top corners of NWs, indicating that the electric field is strongly bounded to the Ag/air interface without noticeable penetration into the ITO layer. This promising feature leads to a strongly asymmetrical optical absorption as mentioned previously. Under such a specific optical property, very few hot electrons are generated in ITO, leading to a neglectable reverse electron flow from ITO to the cladding Ag layer.

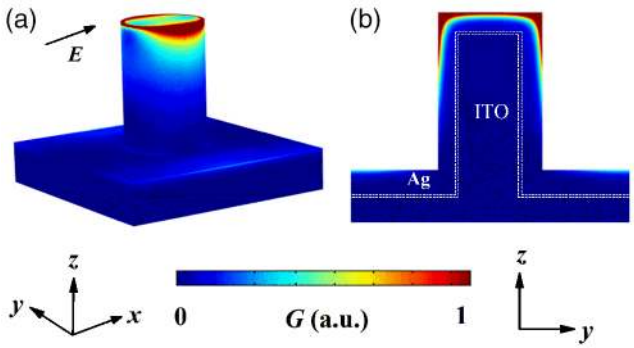


**Fig. 3** (a) The 3-D spatial and (b) corresponding 2-D cross-sectional (in the $yz$ plane) distributions of the hot electron generation rate $G$ in the conformal NWs.

The optoelectronic response of the conformal NWs hot-electron photodetector can be predicted by addressing the detailed transport process of the generated hot electrons inside the photodetection system. However, it is very challenging to conduct a thorough 3-D electronic simulation for the conformal and multilayered NW array system by mimicking the microscopic processes such as the hot-electron diffusion and tunneling . However, a reasonable compromise is to simplify the calculation by cutting the 3-D system into many 2-D cross-sections (through the central axis of the NW), and the overall electrical performance takes the spatial integration.[28] Such a discretization treatment can well approximate the actual response of the 3-D device as long as the number of cross-sectional planes is large enough. In this study, planes with an angular separation of 5 deg are used, i.e., 72 planes in total.

Based on the assumption of an isotropic initial momentum distribution of hot electrons,[29] the probability that a hot electron ballistically reaches the M/S interface without losing energy in an inelastic collision can be expressed by considering the mean free-path (MFP) of hot electrons in solids[30]

$$P_1 = \frac{1}{2\pi}\int_{\theta_1}^{\theta_2} \exp\left(-\frac{d}{\lambda_e \cos\,\theta}\right) \mathrm{d}\theta, \tag{2}$$

where $\theta$ is the moving angle, $\theta_1$ and $\theta_2$ are the accepting angles (i.e., only the hot electrons confined which are possible to reach the M/S interface), $d$ is the distance from the initial position of hot electrons to the M/S interface, and $\lambda_e$ is the MFP of an electron in Ag. To calculate $P_1$, each cross-sectional plane is divided into several sections.[10] The spatial distribution of $P_1$ in a given plane, e.g., with an angle of 30 deg to the $y$ axis, is shown in Fig. 4(a), where only the conformal Ag cladding is considered since the hot electron generations in ITO can be neglected

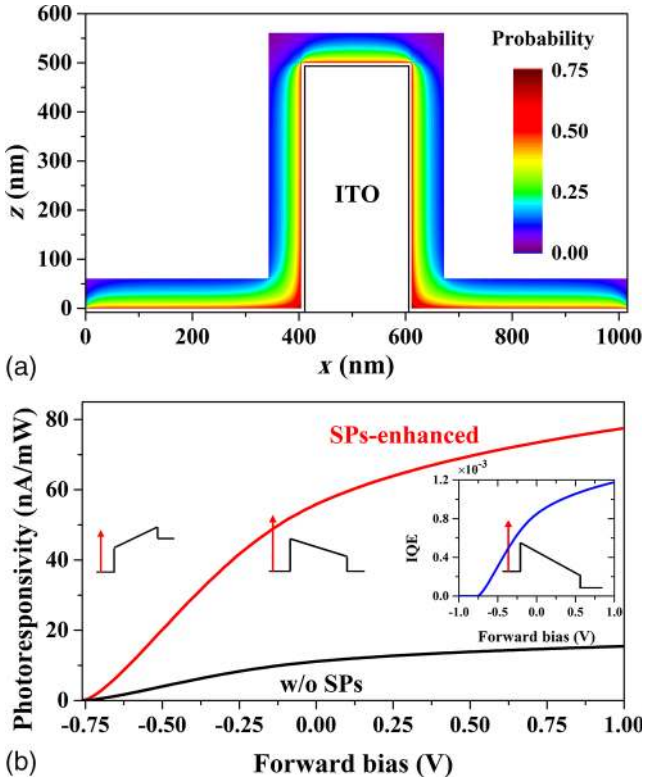


**Fig. 4** (a) Probability of hot electrons in the Ag cladding to successfully arrive at the M/S interface, where a specific cross-section is selected. (b) Photoresponsivity as a function of the forward electrical bias. The IQE versus the forward electrical bias and the corresponding band diagrams at reverse/zero/forward voltages are inserted.

as mentioned above. It can be clearly seen that: (1) high probabilities with the peak value of 0.75 appear at the bottom inner corners of the Ag cladding layer, which is the result of the large accepting angle (270 deg) for electrons to diffuse to the interface; (2) at the inner edges near the M/S interface, the probability is close to 0.5 and decreased gradually with increasing the distance away from the interface under a longer diffusion distance and a smaller accepting angle.[31] From this point of view, using a thinner Ag surrounding layer to excite the localized SPs facilitates the hot electrons to successfully diffuse to the interface for the photocurrent generation.

The transmission probability for hot electrons to tunnel through the ultrathin semiconductor intermediate layer and be collected by the bottom contact is described by considering the underlying physical processes such as the reflections between two interfaces, the scattering loss during the traversal through the semiconductor. The detailed description of the transport process and the corresponding general model can be found in Ref. 9, which has been proved to be accurate enough to show a good consistence to the experiment. The internal quantum efficiency (IQE) can then be obtained by the probability of hot electrons that tunnel through the barrier ($P_2$), propagate through the semiconductor ($P_3$), and transmit into the bottom contact ($P_4$) with the assumption of a constant density of states for the excited electrons

$$\eta_{\mathrm{i}} = \frac{1}{E_{\mathrm{ph}}} \int_{\varphi_B}^{E_{\mathrm{ph}}} P_2 P_3 P_4(E) \mathrm{d}E, \tag{3}$$

where $E_{\mathrm{ph}}$ is the incident photon energy. Because the quantity of $P_2$ and $P_4$ is different for each energy $E$ above the Fermi level of the metal, which ranges from 0 to $E_{\mathrm{ph}}$. In addition, $P_4$ is also affected by the applied voltage. So we take $E = E_{\mathrm{ph}}$ and unbiased case for an example. According to the general formulas in the ESI of Ref. 9, $P_2 = 0.0165$, $P_4 = 0.2375$. The $P_3$ can be estimated with the mean free path of electrons in ZnO ($l_{ox}$) to be $\exp(-\frac{4\ \mathrm{nm}}{l_{ox}}) \approx 1$.[32]

With the spatial distribution of hot electron generation, the probability to reach the M/S interface and the IQE, we can calculate the total photocurrent and the photoresponsivity. Figure 4(b) plots the calculated photoresponsivity of the hot-electron photodetectors as a function of the electrical bias. It is shown that the unbiased photoresponsivity of the device is as high as 56 nA/mW, which is more than five times larger than that of the planar reference (11 nA/mW according to our calculation). To further improve the photoresponsivity, a forward electric bias can be applied, where the positive terminal is connected to the bottom ITO contact and the negative to the Ag cladding. With a bias of 0.8 V, the photoresponsivity is shown to be up to 75 nA/mW, which is attributed to the promoted kinetic energy of hot electrons in the semiconductor (results in a higher transmission probability as shown in the inset).[32] The responsivity of ~80 nA/mW is ~2 times of that based on the multilayered conformal grating system.[10] In addition, it is comparable to that of the plasmonic NWs with a Schottky/Ohmic interface and the optimized plasmonic-crystal-hot-electron-based Schottky photodetectors.[11,33] However, the reverse bias greatly degrades the performance due to the elevated barrier height, preventing electrons from tunneling through the barrier.[9] When the reverse bias is large enough to satisfy the condition that: $|V_{\mathrm{app}}| > (E_{\mathrm{ph}} - \Phi_{\mathrm{B}})/e$, few hot electrons can tune through the barrier. Here, $E_{\mathrm{ph}} = 1.36$ eV, $\Phi_{\mathrm{B}} = 0.6$ eV, so the onset voltage is thus expected to be 0.76 eV, as seen in Fig. 4(b).

Next, as the NW depth is an important parameter to consider, we investigate the effect of the NW depth on the optical performance of the device. Fixing NW period $\Lambda$ and ITO core radius $r$ at 880 and 100 nm, respectively, the optical absorption spectral of $P_{\mathrm{Ag}}$ as a function of the NW depth from 300 to 700 nm are illustrated in Fig. 5(a). It is apparent that the optical absorption in Ag can be improved with the increase of height from 300 to 500 nm. The largest value can be achieved at $H = 500$ nm. Further increasing the height, the light coupling effects are weakened, leading to a decreased absorbance. In addition, the resonances redshift as the height increases.

Finally, since the fabricated structure usually have rounded corner depending on the dimension, the rounded corners of different fillet radius ($fr$) are considered in the NWs. Figure 5(b) shows the effect of the rounded corner on the optical absorption in Ag. It is clear that the

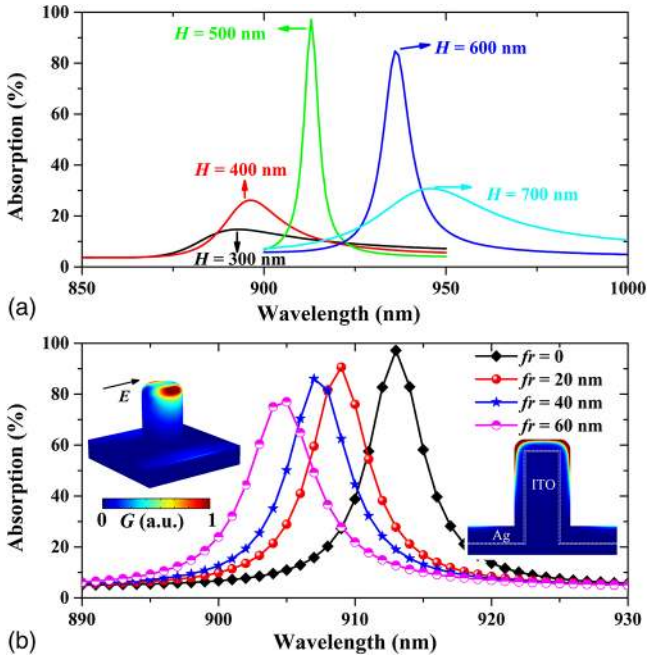


**Fig. 5** Absorption spectra of $P_{Ag}$ under different NW height (a) fillet radius (b) in the fabricated conformal NWs with $r = 100$ nm and $\Lambda = 880$ nm. The insets in (b) are the 3-D spatial distribution and the corresponding cross-sectional distribution of $G$ in the $yz$ plane.

resonance blue-shifts and the peak absorption is slightly decreased as the fillet radius increases, showing a fabrication tolerance. For example, at $fr = 60$ nm, the peak absorption is 77%, which is decreased by ~20% comparing to that of the sharp corner ($fr = 0$). In addition, the 3-D spatial distribution and the corresponding cross-sectional distribution of $G$ in the $yz$ plane are illustrated in the inset with the same scale as that in Fig. 3. Same as that of the NWs with sharp corner, a strong field concentrates at the top corners of NWs, which claims that the rounded corner has little effect on the absorption distribution.

## 4 Conclusion

In summary, we have presented the design of a narrowband, tunable, and polarization-insensitive hot-electron photodetectors by introducing the conformal TCO/S/M NW array configuration. It is found that the plasmonic resonance as well as the corresponding strength and bandwidth can be readily tailored by the lattice periodicity and NW core radius. The detection wavelength under plasmonic resonance is shown to be tuned from the visible to NIR band. At the plasmonic resonance, more than 97% of incident light is absorbed by the surrounding Ag layer, leading to a strong and highly asymmetrical optical absorption between the two contacts and enabling a high unidirectional photocurrent. The spatial distribution of hot electron generation rate suggests a strong field localization at the top corners of the NWs, attributed to the excitation of the localized SPs. By addressing the detailed hot-electron transport process inside the device, it is predicted that the unbiased photoresponsivity can be up to 56 nA/mW, which is more than five times of that based on the planar reference.

## Acknowledgments

This work was supported by PhD Programs Foundation of Ministry of Education of China (20133201110021), Natural Science Foundation of Jiangsu Province of China (BK20141200), the Youth 973 Program (2015CB932700), Thousand Young Talents Program of China, and Priority Academic Program Development (PAPD) of Jiangsu Higher Education Institutions.

## References


1. M. W. Knight et al., "Photodetection with active optical antennas," *Science* **332**(6030), 702–704 (2011).
2. K. Ueno et al., "Plasmon-enhanced photocurrent generation and water oxidation from visible to near-infrared wavelengths," *NPG Asia Mater.* **5**, e61 (2013).
3. M. W. Knight et al., "Embedding plasmonic nanostructure diodes enhances hot electron emission," *Nano Lett.* **13**(4), 1687–1692 (2013).
4. A. Sobhani et al., "Narrowband photodetection in the near-infrared with a plasmon-induced hot electron device," *Nat. Commun.* **4**, 1643 (2013).
5. K.-T. Lin et al., "Silicon-based broadband antenna for high responsivity and polarization-insensitive photodetection at telecommunication wavelengths," *Nat. Commun.* **5**, 3288 (2014).
6. W. Li et al., "Metamaterial perfect absorber based hot electron photodetection," *Nano Lett*. **14**(6), 3510–3514 (2014).
7. I. Goykhman et al., "Locally oxidized silicon surface-plasmon Schottky detector for telecom regime," *Nano Lett.* **11**(6), 2219–2224 (2011).
8. F. Wang et al., "Plasmonic energy collection through hot carrier extraction," *Nano Lett.* **11**(12), 5426–5430 (2011).
9. H. Chalabi et al., "Hot-electron photodetection with a plasmonic nanostripe antenna," *Nano Lett.* **14**(3), 1374–1380 (2014).
10. K. Wu et al., "Strong and highly asymmetrical optical absorption in conformal metal-semiconductor-metal grating system for plasmonic hot-electron photodetection application," *Sci. Rep.* **5**, 14304 (2015).
11. F. P. García de Arquer et al., "Large-area plasmonic-crystal–hot-electron-based photodetectors," *ACS Photonics* **2**(7), 950–957 (2015).
12. D. A. Kovacs et al., "Photo and particle induced transport of excited carriers in thin film tunnel junctions," *Phys. Rev. B* **76**, 235408 (2007).
13. J. B. Chou et al., "Broadband photoelectric hot carrier collection with wafer-scale metallic-semiconductor photonic crystals," in *42th IEEE Photovoltaic Specialist Conf.*, New Orleans, (2015).
14. E. W. McFarland et al., "A photovoltaic device structure based on internal electron emission," *Nature* **421**(6923), 616–618 (2003).
15. C. Clavero, "Plasmon-induced hot-electron generation at nanoparticle/metal-oxide interfaces for photovoltaic and photocatalytic devices," *Nat. Photonics* **8**(2), 95–103 (2014).
16. J. Li et al., "Plasmon-induced photonic and energy-transfer enhancement of solar water splitting by a hematite nanorod array," *Nat. Commun.* **4**, 2651 (2013).
17. S. Mukherjee et al., "Hot electrons do the impossible: plasmon-induced dissociation of $H_2$ on Au," *Nano Lett.* **13**(1), 240–247 (2013).
18. P. J. Schuck, "Nanoimaging: hot electrons go through the barrier," *Nat. Nanotechnol.* **8**(11), 799–800 (2013).
19. A. Giugni et al., "Hot-electron nanoscopy using adiabatic compression of surface plasmons," *Nat. Nanotechnol.* **8**(11), 845–852 (2013).
20. A. Y. Polyakov et al., "Electrical characteristics of Au and Ag Schottky contacts on n-ZnO," *Appl. Phys. Lett.* **83**(8), 1575–1577 (2003).
21. H. Kim et al., "Silver Schottky contacts to a-plane bulk ZnO," *J. Appl. Phys.* **108**(7), 074514 (2010).
22. E. D. Palik, *Handbook of Optical Constants of Solids*, Academic Press, Orlando (1985).
23. Comsol multiphysics, "COMSOL," http://www.comsol.com/ (20 April 2016).
24. E. Prodan et al., "A hybridization model for the plasmon response of complex nanostructures," *Science* **302**(5644), 419–422 (2003).
25. Y. Zhan et al., "Coaxial Ag/ZnO/Ag nanowire for highly sensitive hot-electron photodetection," *Appl. Phys. Lett.* **106**(8), 081109 (2015).
26. X. Li et al., "Extremely high sensitive plasmonic refractive index sensors based on metallic grating," *Plasmonics* **5**(4), 389–394 (2010).

27. T. Gong et al., "Angle-independent hot carrier generation and collection using transparent conducting oxides," *Nano Lett.* **15**(1), 147–152 (2015).
28. Z. Yang et al., "High-efficiency photon capturing in ultrathin silicon solar cells with front nanobowl texture and truncated-nanopyramid reflector," *Opt. Lett.* **40**(6), 1077–1080 (2015).
29. C. Scales et al., "Thin-film Schottky barrier photodetector models," *IEEE J. Quantum Electron.* **46**(5), 633–643 (2010).
30. M. P. Seah et al., "Quantitative electron spectroscopy of surfaces: a standard data base for electron inelastic mean free paths in solids," *Surf. Interface Anal.* **1**(1), 2–11 (1979).
31. K. Wu et al., "Surface-plasmon enhanced photodetection at communication band based on hot electrons," *J. Appl. Phys.* **118**(6), 063101 (2015).
32. Y. Zhan et al., "Infrared hot-carrier photodetection based on planar perfect absorber," *Opt. Lett.* **40**(18), 4261–4264 (2015).
33. B. Y. Zheng et al., "Distinguishing between plasmon-induced and photoexcited carriers in a device geometry," *Nat. Commun.* **6**, 7797 (2015).

**Cheng Zhang** received his BE degree from Soochow University in 2013. He is now a PhD student in the School of Optoelectronic Information Science and Engineering, College of Physics, Optoelectronics and Energy, Soochow University. His research interests include the high-performance hot-carrier photodetection application and advanced light trapping designs for nanostructured solar cells and photoconversion devices. He has published around 10 papers in journals including *Nano Energy, Scientific Reports, Optics Express, Nanoscale Research Letters,* and so on.

**Xiaofeng Li** received his BE and PhD degrees from Southwest Jiaotong University with 5 years' experience in Nanyang Technological University and Imperial College London. He joined Soochow University as a professor since 2012 and become the deputy dean since 2014. He focuses on photovoltaics and photodetections with ~100 publications. He is the recipient of "Thousand Young Talents Program" of China and an IEEE senior member. He is currently a topical editor of *Applied Optics*.

Biographies for the other authors are not available.